Zone-Based Positioning Using Trust Beacons, Angle Diversity, and Optical Wireless Communications

E.W. Lam and T.D.C. Little
Electrical and Computer Engineering Department, Boston University, Boston, MA USA
{*emilylam, tdcl*}*@bu.edu*

***Abstract*—We propose a new indoor positioning paradigm called zone-based positioning in which angle-diverse optical user-devices position themselves with respect to low-cost, fixed-location, active photovoltaic anchors. Due to the low cost, these anchors, called trust beacons, are distributed liberally throughout a space. This distribution of beacons enables a mobile positioning zone that travels with a particular user-device as it moves through space. Privacy is maintained by distributing the active components between the user device and infrastructure. To ensure real-time measurement of angle and range, a narrow field-of-view optical source is continuously modulated with updated measurements. We demonstrate mean square errors of less than 20cm for 2D positioning and less than 5cm for light detection and ranging (LIDAR) assisted 3D positioning. We also demonstrate an experimental proof-of-concept prototype.**

***Index Terms*—Visible Light Positioning, Light-based Positioning, Optical Wireless Communications, Location-based Services, Zone-based Positioning, ZPS**

I. Introduction

Seamless, adaptable, and continuous positioning is the next frontier for indoor positioning and localization. However, the indoor environment is neither homogeneous in space nor in use-case and is thus difficult to cover with a single positioning technology. Possible modalities that satisfy different contexts, resolutions, and scenarios include: radio frequency (RF), light, ultrasound, and imaging. Moreover, a contemporary tracked device is likely different in device type and freely moves across changing spatial domains. Thus, an opportunity exists for a lightweight solution that can easily adapt to different scenarios.

Along with high accuracy and low cost, privacy preservation is another important and desirable feature in modern positioning solutions. One way to accommodate privacy-preservation is to let the user decide to participate or not. This criterion requires teasing out and isolating the active elements of the positioning system from the user device and the infrastructure. For example, with GNSS, a user decodes received signals privately by choice enabled by the active antennas within the device. In juxtaposition, camera-based positioning infrastructure can work passively without negotiation with a user device.

Recent literature shows that angle diversity schemes (angle-of-arrival – AOA) and time synchronized positioning systems provide the best results for indoor positioning regardless of medium [1], [2]. Systems that use timing-based schemes (time-of-flight/time-difference-of-arrival – TOF/TDOA) can be very accurate, but the need for time synchronization makes them hard to implement across large number of devices and spaces [3]. Commercial ultra-wideband (UWB) and motion capture camera systems provide great accuracy at the expense of system-level knowledge of position (less privacy) [3]. Light-based positioning is inherently directional and works well with AOA approaches. Recent efforts in literature have been committed toward developing new AOA receivers for two-party bistatic systems, that is, systems that are infrastructure-based with active devices that locate themselves. These receivers can require numerous apertures [4], rotating mechanisms [5], or structured tilts [6] and are not ideal from a cost and implementation perspective for large number of devices. Increasing angle diversity at the transmitters is also an option [7]–[9].

Concurrently, the future of mobile devices is also changing: the Cisco VNI Mobile Forecast and Trends estimates that by 2022, there will be 1.1 billion wearable devices globally [10]. Fueled by 5G and edge communications, an emerging market within wearables includes head-mounted devices for augmented and virtual reality (AR/VR), audio listening, and video recording. These include commercial entities such as Microsoft HoloLens (AR), Bose Frames (audio), Snap Spectacles (camera), and others. We believe headsets are forthcoming and design our new positioning technique to leverage positioning paradigms as they would apply to a mobile headset.

Addressing these needs, we propose a positioning approach that extends the useful mobile positioning volume around a user device capable of measuring its angle of departure and transmitting it over a narrow field-of-view (FOV) optical link. We call this new paradigm a Zone-based Positioning Service (ZPS), illustrated in Fig. 1. With ZPS, a positioning unit carried by a person locates a special beacon called a Trust Beacon (TB). The position of the unit is then determined based on its orientation, pointing angles, and optional range received at the TB as an optical payload and TB anchor coordinates.

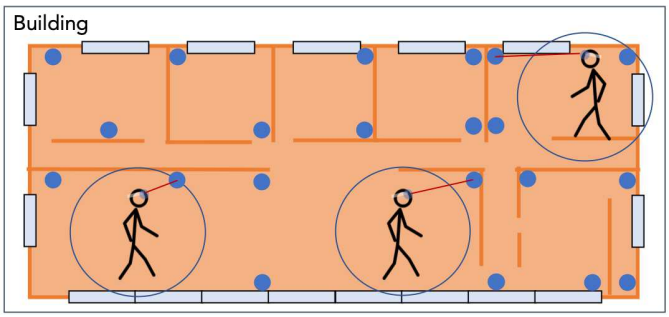

Fig. 1: Zone-based Positioning Service (ZPS)

E. W. Lam and T. D. C. Little, "Zone-Based Positioning using Trust Beacons, Angle Diversity, and Optical Wireless Communications," 2020 IEEE International Conference on Communications Workshops (ICC Workshops), Dublin, Ireland, 2020, pp. 1-6, doi: 10.1109/ICCWorkshops49005.2020.9145095.

The positioned unit acquires the relevant data from the TB via an RF backhaul. ZPS fuses three core technologies in a novel way: active anchors, angle diversity, and optical wireless communications (OWC). Finally, ZPS deliberately contains location data for privacy-preservation.

The remainder of the paper is organized as follows: Section II proposes the Zone-based Positioning Service in detail; Section III describes a system design and implementation of ZPS; Section IV discusses simulated and experimental results; and finally, Section V concludes the paper.

II. Zone-based Positioning Service

With the Zone-based Positioning Service, user-devices (UDs) anchor and position themselves with respect to the surrounding environment. The infrastructure is aware that the user is within the space but not where the user is in the space. This is similar to access point (AP) technology in which an AP is aware of the presence of active devices within its scope, but not the locations of the devices. By maintaining this level of privacy, exact user position data harvesting is avoided.

To accomplish positioning with this archetype, we embrace technologies that are low-cost, readily available, and distributed between the user and infrastructure. At the infrastructure side are fixed location active devices called Trust Beacons that are self-aware of their respective locations within a building or space. At the user-end is a headset consisting of an inertial measurement unit (IMU), a low-power laser diode for OWC, amongst other things, called the Zone-Positioning Unit (ZPU).

A. Trust Beacons

Trust beacons create the backbone of ZPS. TBs are fixed location beacons commissioned with knowledge of their respective coordinates so that they are self-aware of their locations. They also contain photovoltaic elements and RF communications for respectively decoding optical communications and backhaul systems communications. Because of its role of position fixing (nulling accumulated position drift error) and orienting, we would ideally place TBs throughout a navigated space but also with higher frequency in areas in which higher precision positioning is desired. Thus the physical design of a TB is intended to be simple and inexpensive, comprised of a simple RF-enabled microcontroller (MCU) with a photodiode (PD) optical receiver. Inexpensive components let us proliferate TBs throughout a space at a low system cost. Note that the TBs are designed to operate in either hierarchical or peer-to-peer (P2P) mode without continuous connection to a broader network. This characteristic is an additional advantage to enhancing location privacy in the proposed system. In addition, the TBs can work with a range of ZPUs of varying complexities to enable different performance levels. By making the TBs simple and reusable, the TB infrastructure allows for integrative rollout of positioning based on need.

B. Zone-Positioning Unit

The ZPU is the target UD that positions itself by using angle-of-departure and ranging to estimate its position in 2D or 3D. The ZPU can be a headset worn on the user consisting at minimum of a MCU, IMU, and wireless narrow FOV optical link. By requiring active communications, the target device can control when positioning occurs. This is in contrast to other schemes, such as the use of cameras, that can continuously track users or UDs.

For robustness, some of these components have opportunities for improvement. One is with the acquisition efficiency of the TB by the ZPU. Steerable micro-electromechanical system (MEMS) mirror elements [11] and gaze-tracking [12], where the laser is steered with feedback from gaze-tracking, can be added for speedy target acquisition; a cursory glance at a TB can result in TB acquisition. MEMS beam steering also allows for higher angle resolution and the ability to rapidly scan a space. In addition, if user height is unknown – the 3D case – a ranging unit can be used to obtain that necessary dimension. In the system highlighted in Fig. 2, we have included an optional light detection and ranging (LIDAR) device as this ranging unit, but any other ranging unit can be chosen for varying results and accuracies (e.g., received-signal-strength (RSS) ranging of: light, RF, sound, TOF sensors, etc.).

C. Communications and Positioning

A key distinguishing element in ZPS is the episodic communications between the ZPU and a TB. The initial communications is accomplished using a narrow FOV optical link (i.e., a low-power laser). In our system, this optical link is visible or infrared and can be steered for a wider coverage using MEMS steering [11], [13]. The optical communications link is unidirectional from headset to beacon. Within the laser communications payload are the current orientation of the ZPU, range information if present, and instructions on how to communicate back to the ZPU via an RF backchannel. Once the TB receives the payload, it relays a message back to the ZPU with the orientation angles it receives and with its own coordinates appended. Finally, the ZPU computes position using the TB coordinates, measured angles, and ranges.

The laser is continually modulated so that whenever the laser hits a target TB receiver, the TB can initiate the return messaging and the ZPU can position itself with the new information provided by the TB. The line-of-sight (LOS) nature of the laser beam allows the beam to be treated as a ray in models, which means the angle of departure is the key captured data. With regards to laser intensity and modulation, the payload is relatively small that on-off-keying (OOK) at low intensities is sufficient. We have shown this form of laser modulation in our ray-surface implementation [14]. In the

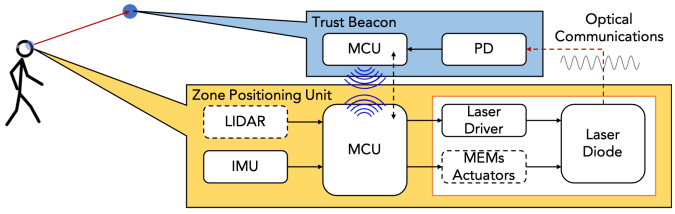

Fig. 2: The Zone-based Positioning Service: Trust Beacons and Zone-Positioning Units

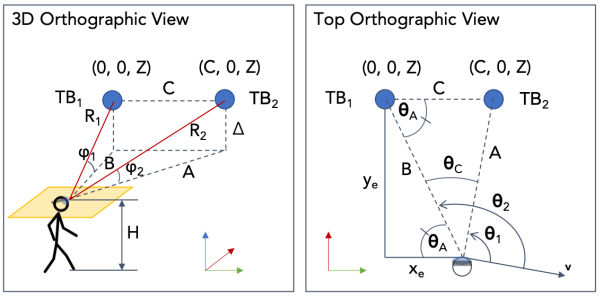

Fig. 3: Orthographic Geometry Between a ZPU and Two TBs

case where LIDAR is used for ranging, the laser payload can be designed to accommodate LIDAR pulses or an additional LIDAR unit is colocated with the laser.

III. System Design and Implementation

In this section, we describe the system design, geometric models, and a proof-of-concept prototype used to evaluate the proposed ZPS.

A. Estimating Position

1) 2D Positioning: As a baseline, we model the 2D scenario, in which the user height is assumed known. Measured values at the ZPU headset are pitch and yaw angles: ϕ_i and θ_i, where i refers to TB_i. When subjected to uniform noise, pitch and roll become: $\hat{\phi}_i = \phi_i + \phi_n$ and $\hat{\theta}_i = \theta_i + \theta_n$. We assume roll is negligible as the headset will sit symmetrically on the head of a person. Due to no prior reference heading direction, since θ_i is measured from a fixed but unknown vector, $\mathbf{v}$, we use two TBs, placed C away from each other laterally, shown in Fig. 3, to calibrate yaw. Pitch and roll are respective to the horizon and thus can be pre-calibrated. From the pitch angles, known user height, H, and beacon coordinates based on the geometry described in Fig. 3, we can estimate the planar distances between the user and TBs, A and B:

$$B = \frac{|\Delta|}{tan(\phi_1)},\ A = \frac{|\Delta|}{\tan(\phi_2)}, \tag{1}$$

where $\Delta = H - Z$ and Z is the z-coordinate of the TBs.

To estimate position, we next resolve the orientation yaw aspect of the headset. Thus, we designate the angle difference between the beacons as $\theta_C = \theta_2 - \theta_1$. We then use the Law of Sines to calculate angle, θ_A:

$$\theta_A = sin^{-1}\left[\frac{Asin(\theta_C)}{C}\right]. \tag{2}$$

Although C is defined and known, confining C may actually force ΔABC to not converge resulting in no triangle solution possible from the measured data. In that case, we can also estimate C as $\hat{C}$ using the Law of Cosines:

$$\hat{C} = \sqrt{A^2 + B^2 - 2ABcos(\theta_C)}. \tag{3}$$

This allows for a solved triangle every time with the measured data, albeit sometimes with greater or lesser errors. We explore the effects of using C versus $\hat{C}$ in the results section as they affect errors based on TB placement.

Finally, from θ_A, we estimate $\hat{x}, \hat{y}$, with respect to TB_1:

$$\hat{x} = Bcos(\theta_A),\ \hat{y} = Bsin(\theta_A). \tag{4}$$

2) 3D Positioning: For the 3D scenario, when height is unknown, another measurement in the form of range is required. Although we configure our system for LIDAR, range information can be provided in a multitude of ways with different accuracies: light and RF ranging via RSS, RADAR, TOF, etc. We use specifications from a consumer-grade Class 1 LIDAR device for our simulations – the Garmin LIDAR-lite has an accuracy of $\epsilon_R = \pm 2.5cm$. With LIDAR, radial distance between TB and user, R_i is measured, where i refers to TB_i. A and B are now calculated from R_1 and R_2:

$$B = R_1cos(\phi_1), A = R_2cos(\phi_2). \tag{5}$$

Now, we can calculate for height using Equation 1:

$$\hat{z}_1 = Z - Btan(\phi_1),\ \hat{z}_2 = Z - Atan(\phi_2). \tag{6}$$

We can average the two values together for a better height estimate. In fact, we can average any number of beacon measurements encountered for height improvements over time:

$$\hat{z}_i = Z - R_isin(\phi_i), \tag{7}$$

$$\hat{z} = \frac{1}{N}\sum_{i=1}^{N}\hat{z}_i, \tag{8}$$

where N is the total number of beacons with measurement data, and R_i is the radial distance between TB_i and the ZPU measured with a ranging sensor, and ϕ_i is the angle related to the radial distance measured by the IMU.

B. Experimental Setup

Fig. 4 shows the experimental prototype ZPU headset with the 5mW 650nm red TTL–transitor-transitor logic–laser (Adafruit part no. 1056), and laser driver (Adafruit variant ESP32 MCU – fitted to a pair of Bose Frames. The Bose Frames is a commercial-off-the-shelf (COTS) audio AR headset with built-in motion sensors: an accelerometer, gyroscope, and magnetometer. The Bose Frames API uses these sensors to compute a quaternion that converts to Euler angles: pitch, roll, and yaw. Fig. 4 shows the these reference rotation axes. We drive the laser using the UART communication protocol, which is a simple OOK modulation common with MCUs, at a modest baud rate of 115.2kbps as speed is not our concern in this paper. However, OWC literature show Gbps data rates [15]. The trust beacon is implemented using a Thorlabs PIN PD (part no. PDA36A) with another ESP32 MCU.

As for the test harness, we mount the prototype ZPU on an optical breadboard for stability, which in turn is fastened to a sturdy tripod, Fig. 5. The tripod enables adjustment of height, pitch, and yaw reliably and quickly. The entire setup is placed within the coverage of a motion capture camera system (Optitrack) to measure the coordinates of the ZPU down to millimeters. The TBs are placed on a cage as shown in Fig. 5.

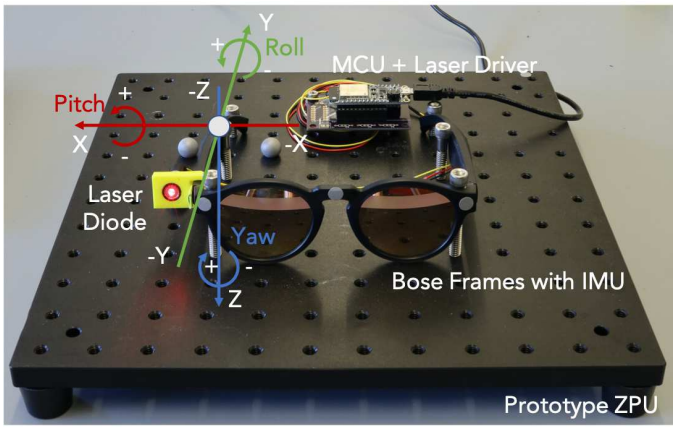

Fig. 4: Prototype ZPU with Reference Axes: Pitch, Roll, Yaw

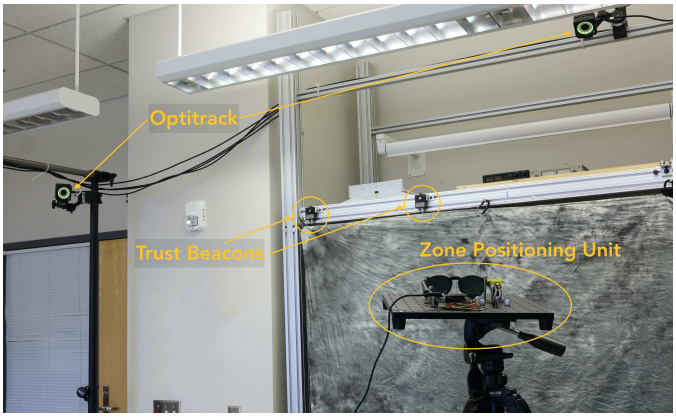

Fig. 5: Experimental COTS Test Apparatus: TBs and ZPU

C. Sources of Errors

The headset used (Bose Frame) comes with no specification for the accuracy of its sensors. For supporting accurate positioning we are particularly concerned about the repeatability of measurements taken after various translations and rotations of the device. Experimentation reveals that in the case of a fixed position (no motion), the device reveals consistent measurements in returned pitch, roll and yaw. We also experiment to measure the drift of the reported pitch, roll, and yaw when exposed to motions confined to movements less than 10m from starting location and accelerations less than 9.8m/s^2 (gravity). These are achieved as follows.

First, we measure the pitch, roll, and yaw of the device at a known location. Next, we move the Bose Frames erratically (e.g., motion that is jerky, smooth, quick, elaborate, small, large, etc.) and place the device back at the known location and remeasure the pitch, roll, and yaw angles. We repeat this procedure for 20 samples. Fig. 6 shows the raw measured angles. We find that with pitch and roll, the measurements remained consistently within $\pm 0.5^\circ$ of the mean, whereas with yaw, the measurements drift upwards. This is due to pitch and roll measured relative to gravity and the horizon and yaw having no reference point. We can combat the lack of a yaw reference by calibrating between two points. Fig. 6 shows that when we take the difference between two yaw measurements, by rotating the device between two known locations, the angle differences between the measurements are now consistent with the pitch and roll measurements and within $\pm 0.5^\circ$ of the mean. This experiment gives us confidence to to use the θ_C measurement mentioned in Section III-A for position estimates. We also use this ± 0.5 error as noise, ϕ_n, θ_n, in our simulations.

We can increase yaw accuracy by using the yaw angle difference of a MEMS steerer, which can bring the noise error to less than 0.01°, which we explore in the results section. Finally, it is possible to reference magnetic north using the magnetometer but that technique is not reliable indoors. There are also higher-end IMUs and different algorithms beyond the COTS Bose Frame system for calculating pitch and yaw.

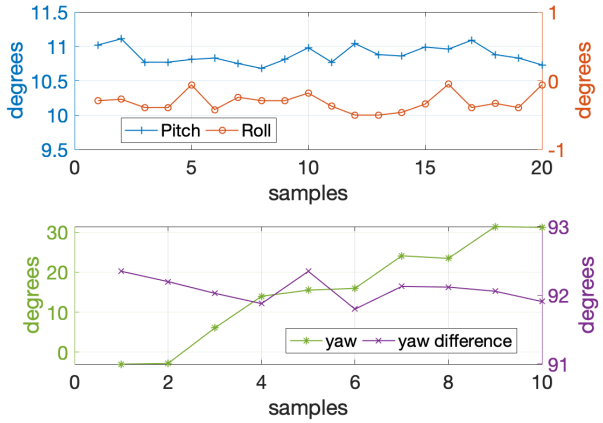

Fig. 6: Repeatability Analysis Shows Consistent Measurements within $\pm 0.5^\circ$ of Mean for Pitch, Roll, Yaw Difference

IV. Results

In this section, we consider both simulated and experimental setups to investigate different configurations of ZPS and compare to other light-based AOA approaches. The conditions simulated explore the effects of different configurations such as the use of MEMS steering and different TB placement locations. The experimental parameters show performance using COTS components. Table I summarizes these parameters, where not previously defined parameters X and Y are the test coordinate locations.

TABLE I: Simulation and Experimental Parameters

Parameter	Baseline	with MEMS	Experimental
TB_1	(0, 0, Z)m	(0, 0, Z)m	(0, 0, Z)m
TB_2	(C, 0, Z)m	(C, 0, Z)m	(C, 0, Z)m
ϕ_n	0.5°	0.5°	∼0.5°
θ_n	0.5°	0.01°	∼0.5°
ϵ_R	0.025m	0.025m	0.025m
H	1.654m	1.654m	1.654m
X	[1:0.1:2]	[1:0.1:2]	[1:0.1:2]
Y	[1:0.1:2]	[1:0.1:2]	[1:0.1:2]

A. 2D Positioning Errors

Here we discuss 2D errors for both simulated and experimental setups. For test coordinates, we choose a 1m ×

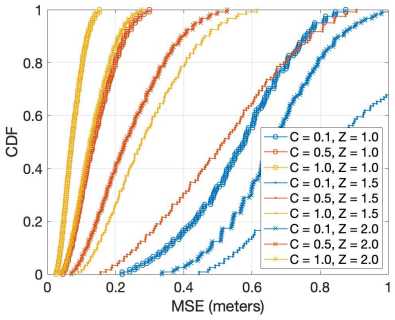

(a) 2D Errors: Effects of TB Height Placement, Z, and Lateral Displacement, C

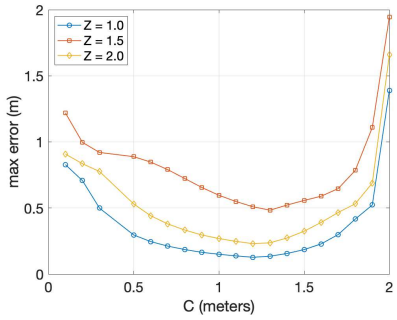

(b) 2D Errors: Max MSE for C = 0.1m to 2.0m and θ_e = 0.01°

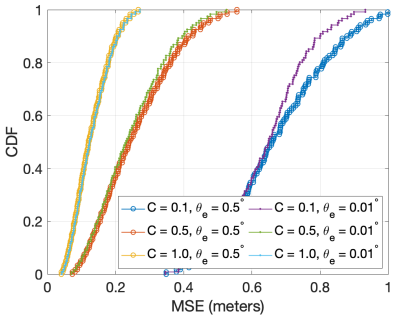

(c) 2D Errors: Comparing Angle Resolutions for Different Lateral Displacements

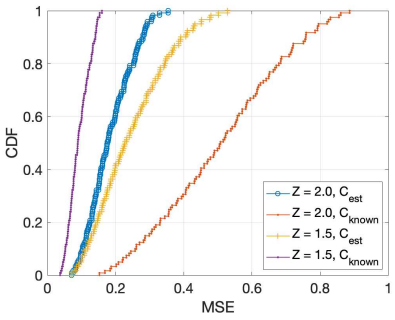

(d) 2D Errors: Effects of Estimating Using C Versus $\hat{C}$ at Different TB Heights

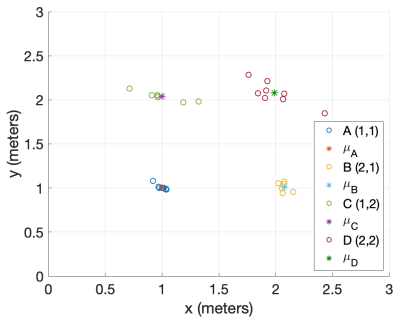

(e) 2D Errors: Experimental Proof-of-Concept Results with COTS Components

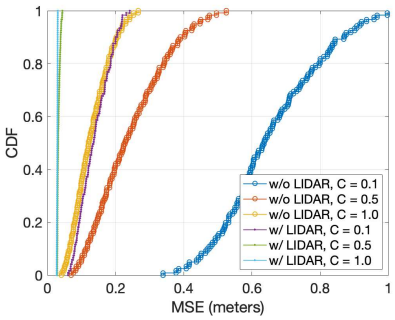

(f) 3D Errors: LIDAR-Assisted and Using Estimated Displacement, $\hat{C}$

Fig. 7: (a)-(d): Simulated 2D Errors, (e) Experimental 2D Errors, and (f) Simulated 3D Errors

1m plane at least 1m away from TB_1 in both x and y dimensions. This assumption is based on the ZPU unlikely being at large angles away from the TBs in normal uses. The user height is assumed fixed for all results at 1.654m which is an approximate average human height.

Fig. 7a explores estimated position estimates as a cumulative distribution function (CDF) of the mean square error (MSE) for different TB placement heights and also the lateral displacement C between the TBs across the entire test space under the baseline parameters. The note of interest here is that a small C distance results in weaker performance regardless of height. The best performance is when the TB is placed at 1m, a difference of 0.654m away from the user, which illustrates that placing the TBs at a plane not close to human height is ideal. This effect is due to angle measurements having a smaller effect on large angle deviations. Fig. 7b shows different values of C and the maximum error in the test space at different TB heights. Along with proving that a large height difference results in the best performance as concluded with the prior graph, Fig. 7b also shows the optimal C displacement for a given TB height. For around 0.5m to 1.5m displacement, the results are similar with no significant improvement. Placing TBs between 0.5m to 1.5m away from each other is thus ideal.

Fig. 7c shows the difference in finer quality steering when introducing MEMS steering in the yaw axis. The MEMS steering does reduce position estimate errors but not drastically. However, MEMS steering is still desirable for certain use cases as the MEMS actuators provide faster convergence in the form of fast steering speed and a large FOV – a Mirrorcle Scan Module has a scan rate of 1Khz and a FOV of 40°. This is important for mobile devices and use cases requiring fast acquisition of TBs with less effort from the user. Although not studied, MEMS steering can be used for pitch as well. Decreasing the noise on both pitch and yaw will likely result in incremental performance gains.

Fig. 7d shows the difference when using a known TB displacement, C, versus an estimated displacement, $\hat{C}$. Each of C and $\hat{C}$ perform well depending on height. There is no fast holding rule to follow on whether a known or estimated displacement should be used as it is dependent on TB location. Fortunately, TB location is known to the user-device when estimating. However, in the case of uncertainty, $\hat{C}$ will always ensure an estimate can be made and is the better choice for displacement.

Fig. 7e show results using data collected from the proof-of-concept experimental COTS configuration at four different locations: A(1,1)m, B(2,1)m, C(1,2)m, and D(2,2)m and an user height of 1.535m – tripod height. The TBs were placed respectively at (0,0,2)m and (0,0.5,2)m. We also used a small angle approximation as the laser is placed adjacent to the Bose Frames reference axes. Experimental results show that accuracies are location dependent as expected and consistent

with simulations. We found that for location A and B, MSE was less than 15cm. However, for locations C and D, errors are larger. The means at each test point though, μ_A, μ_B, μ_C, and μ_D, have MSE of less than 15cm. Given the limitations of a laboratory setup where the laser is adjacent and not exactly on the ZPU pitch and yaw axes, these results are promising.

B. 3D Positioning Errors

Factoring in range from LIDAR greatly increases the positioning accuracy even though we are adding an additional cost dimension to the positioning system. This is because LIDAR is a high accuracy methodology and provides better estimates for radial distances than estimating based off the IMU: Eq. 1 versus Eq. 5. Fig. 7f show positioning accuracies of less than 5cm under the baseline condition for 3D positioning, which is a vast improvement over the 20cm accuracy for 2D positioning. This accuracy can be further improved with better ranging devices as we used specifications from a consumer hobbyist grade LIDAR device. This makes the ZPU a device that can be designed to come at different cost points. In fact for coarser resolutions or inexpensive devices, the ranging unit can be lower quality than the LIDAR device that we used as a baseline. Since 2D positioning is a special case of 3D positioning with known height, a range sensor based solution can also be used for 2D for better resolutions in 2D.

C. Comparison to Other AOA Approaches

Table II compares two other light-based AOA positioning approaches. With respect to performance, AOA approaches perform comparably on the same order of magnitude. The differentiators are the hardware requirements and complexity to accomplish AOA. Each of the compared techniques have extra peripherals in addition to light. From a computation perspective, cameras require image processing and more computation power. ZPS uses commodity components that are low in computation and also likely to have multiple uses in an UD – most consumer devices already incorporate IMUs and LIDAR units are becoming increasingly common for depth perception. A photodiode structure [4], [6] is also less multipurpose. The TB infrastructure of ZPS is anticipated to be inexpensive as it is just a PD and MCU – these could be built in to internet-of-things (IOT) devices. The dual-purpose of lighting is advantageous for the methods introduced in [4], [6]. However, revolutionizing the lighting industry is harder than introducing new information technology services.

TABLE II: Comparison of Light-based AOA Approaches

Method	Accuracy	Sources/Sinks	Extras
[4]	3.25cm	4 TX/4 PDs	Apertures, Camera
[6]	6cm	1 TX/3 PDs	Tilted PDs
This Paper	5cm	1 TX/2 PDs	IMU, LIDAR

V. Conclusion

We propose a new indoor positioning approach comprised of trust beacons, angle diversity, and a zone positioning unit. In this paradigm, trust beacons serve as smart anchors used to assist in localization of a mobile Zone Positioning Unit. With the ZPU intended as a headset, line-of-sight is not an issue if beacons are placed sufficiently above the heights of humans. The ZPU can also be realized with different technologies including LIDAR and MEMS mirrors to achieve increasing levels of performance. In the various simulated configurations, we demonstrate positioning error bounds of 20cm for 2D positioning and 5cm for LIDAR-assisted 3D positioning. We also demonstrate an initial proof-of-concept implementation using off-the-shelf components. The low cost beacon design makes scaling to large number of different types of user devices feasible and is a long-term solution that is adaptable to future deployments.

References

[1] E. W. Lam and T. D. C. Little, "Visible light positioning: moving from 2D planes to 3D spaces," *Chinese Optics Letters*, vol. 17, no. 3, p. 030604, Mar. 2019.

[2] Y. Zhuang, L. Hua, L. Qi, J. Yang, P. Cao, Y. Cao, Y. Wu, J. Thompson, and H. Haas, "A survey of positioning systems using visible LED lights," *IEEE Communications Surveys Tutorials*, vol. 20, no. 3, pp. 1963–1988, thirdquarter 2018.

[3] M. Tanigawa, J. D. Hol, F. Dijkstra, H. Luinge, and P. J. Slycke, "Augmentation of low-cost GPS/MEMS INS with UWB positioning system for seamless outdoor/indoor positionng," in *Proceedings of the 21st International Technical Meeting of the Satellite Division of The Institute of Navigation (ION GNSS 2008)*, 2008.

[4] S. Cincotta, C. He, A. Neild, and J. Armstrong, "Indoor visible light positioning: Overcoming the practical limitations of the quadrant angular diversity aperture receiver (QADA) by using the two-stage QADA-plus receiver," *Sensors*, vol. 19, no. 4, 2019.

[5] Q.-L. Li, J.-Y. Wang, T. Huang, and Y. Wang, "Three-dimensional indoor visible light positioning system with a single transmitter and a single tilted receiver," *Optical Engineering*, vol. 55, pp. 55 – 55 – 7, 2016.

[6] S. H. Yang, H. S. Kim, Y. H. Son, and S. K. Han, "Three-dimensional visible light indoor localization using AOA and RSS with multiple optical receivers," *Journal of Lightwave Technology*, vol. 32, no. 14, pp. 2480–2485, July 2014.

[7] Lixuan Wang, Caili Guo, P. Luo, and Q. Li, "Indoor visible light localization algorithm based on received signal strength ratio with multi-directional LED array," in *2017 IEEE International Conference on Communications Workshops (ICC Workshops)*, May 2017, pp. 138–143.

[8] E. W. Lam and T. D. C. Little, "Resolving height uncertainty in indoor visible light positioning using a steerable laser," in *2018 IEEE International Conference on Communications Workshops (ICC Workshops)*, May 2018, pp. 1–6.

[9] ——, "Angle diversity to increase coverage and position accuracy in 3D visible light positioning," in *ICC 2019 - 2019 IEEE International Conference on Communications (ICC)*, May 2019, pp. 1–7.

[10] "Global mobile data traffic forecast update, 2017–2022," Cisco Visual Networking Index, Feb. 2019.

[11] V. Milanovic and Wing Kin Lo, "Fast and high-precision 3D tracking and position measurement with MEMS micromirrors," in *2008 IEEE/LEOS International Conference on Optical MEMs and Nanophotonics*, Aug. 2008, pp. 72–73.

[12] M. Kassner, W. Patera, and A. Bulling, "Pupil: An open source platform for pervasive eye tracking and mobile gaze-based interaction," in *Proceedings of the 2014 ACM International Joint Conference on Pervasive and Ubiquitous Computing: Adjunct Publication*, ser. UbiComp '14 Adjunct. New York, NY, USA: Association for Computing Machinery, 2014, pp. 1151–1160.

[13] M. B. Rahaim, J. A. Morrison, and T. D. C. Little, "Beam control for indoor FSO and dynamic dual-use VLC lighting systems," *Journal of Communications and Information Networks*, vol. 2, no. 4, 2017.

[14] E. W. Lam and T. D. C. Little, "Indoor 3D localization with low-cost LiFi components," in *2019 Global LIFI Congress (GLC)*, June 2019, pp. 1–6.

[15] B. Fahs, M. Romanowicz, and M. M. Hella, "A Gbps building-to-building VLC link using standard CMOS avalanche photodiodes," *IEEE Photonics Journal*, vol. 9, no. 6, pp. 1–9, Dec. 2017.